Nano Energy 127 (2024) 109797

Contents lists available at ScienceDirect

Nano Energy

journal homepage: www.elsevier.com/locate/nanoen

Drag force shear manipulating ligand distribution at perovskite buried interface enables efficiently suppressed EQE roll-off of perovskite light-emitting diodes

Qungui Wang [a,b,1], Xiaodong Peng [c,1], Wen Li [c], Xiankan Zeng [c], Yongjian Chen [c], Lunyao Pan [c], Guanqi Tang [a,*], Xiangrong Chen [b,*], Weiqing Yang [a,c,**]

[a] Research Institute of Frontier Science, Southwest Jiaotong University, Chengdu 610031, PR China
[b] College of Physics, Sichuan University, Chengdu 610065, PR China
[c] Key Laboratory of Advanced Technologies of Materials (Ministry of Education), School of Materials Science and Engineering, Southwest Jiaotong University, Chengdu 610031, PR China

ARTICLE INFO

Keywords:
Perovskite light-emitting diode
Buried interface
Nanocrystals
Ligand distribution
Drag force shear

ABSTRACT

Effectively manipulating the ligand distribution at the perovskite buried interface is critical for achieving high-performance nanocrystal-based perovskite light-emitting diodes (PeLEDs). However, it is challenging to realize it due to the non-exposed feature of the buried interface. Here, the drag force shear (DFS) is utilized to successfully regulate the ligand distribution at the perovskite buried interface which can effectively suppress the EQE roll-off of devices. By manipulating the ligand distribution at the perovskite buried interface, it is revealed that a more ligand preservation could result in an improved defect passivation leading to higher EQE, while the carrier injection barrier is increased simultaneously making devices suffer from severe EQE roll-off and decreased luminance, and vice versa. With the help of optimizing the ligand distribution by manipulating the DFS, the balance between carrier injection and interfacial defect passivation is successfully achieved. Resultantly, an enhanced EQE of 17.24 % with substantially suppressed EQE roll-off is reached, culminating in a remarkable luminance of 61,900 cd/m^2. This work presents an efficient approach to control ligand distribution at the perovskite buried interface and offers valuable insights for realizing high luminance and low EQE roll-off of PeLEDs.

1. Introduction

Perovskite light-emitting diodes (PeLEDs) are the rising stars in the next generation of high-performance illumination, displays, and rapid communication devices due to their significant advantages, including high color purity, solution processability, and large-area manufacturability [1–6]. Within a decade, the external quantum efficiencies of red, green, and blue PeLEDs have already reached 25.8 % [7], 30.84 % [8], and 18.65 % [9]; respectively. However, the operational stability of PeLEDs has lagged far behind their rapid development in performance, especially for nanocrystal based PeLEDs [10]. Nowadays, nanocrystal-processed PeLEDs are still suffering from the substantial EQE decline under high current-density conditions, known as EQE roll-off, severely limiting their achievement of high brightness and widespread applications [11,12].

It is well known that the ligand distribution of nanocrystal-based perovskite has critical impact on the PeLED performance [13–16]. Insufficient surface ligand distribution will lead to massive surface defects, resulting in an increase in defect-assisted non-radiative recombination and thus significantly decrease the radiative recombination efficiency of the device. However, excess distribution of surface ligands will increase the carrier injection barrier, which seriously reduces the device luminance and accelerate the EQE roll-off at high current density due to the electrical insulating property of surface ligands [17–25]. Nonetheless, current researches on the treatment of surface ligands are mainly focused on the regulation of ligands during the preparation process of nanocrystals or post surface treatment of perovskite films after the deposition of perovskite film [26–30]. There are few methods

* Corresponding authors.
** Corresponding author at: Research Institute of Frontier Science, Southwest Jiaotong University, Chengdu 610031, PR China.
E-mail addresses: qunguiwang@163.com (Q. Wang), guanqitang13@gmail.com (G. Tang), xrchen@scu.edu.cn (X. Chen), wqyang@swjtu.edu.cn (W. Yang).
[1] These authors contribute equally.

https://doi.org/10.1016/j.nanoen.2024.109797
Received 11 April 2024; Received in revised form 21 May 2024; Accepted 26 May 2024
Available online 27 May 2024

demonstrated to regulate ligand distribution at the perovskite buried interface due to the great difficulty in handling the buried interfaces [31, 32]. Considering the significant importance of the ligand distribution at the perovskite buried interface for the performance of PeLEDs, it is highly desired to develop an efficient strategy to finely tune the ligand distribution at the perovskite buried interface to further improve the device performance and suppress EQE roll-off at high current density for PeLEDs [33–36].

The combination between surface ligands and nanocrystal are dynamic and weak binding because of its ionic nature [37–39], which could be easily sheared by the external forces [40–42]. Herein, we employed a drag force from the relative motion between solution and perovskite nanocrystal during the spin-up stage to efficiently manipulate the ligand distribution of the perovskite buried interface for effectively suppressing the EQE roll-off in high-performance PeLEDs. By directly peeling-off and exposing the perovskite buried interface, we revealed that weaking the drag force shear (DFS) will lead to a more ligands distribution at the perovskite buried interface, resulting in an efficient defect passivation. However, this increased ligand distribution will also significantly heighten the carrier injection barrier at the buried interface. Thus, the weak DFS perovskite based PeLEDs exhibit an evidently improved peak EQE while suffer from a faster EQE roll-off simultaneously. In contrast, strengthening the DFS would reduce the EQE but suppress the EQE roll-off for PeLEDs due to more defects and lower

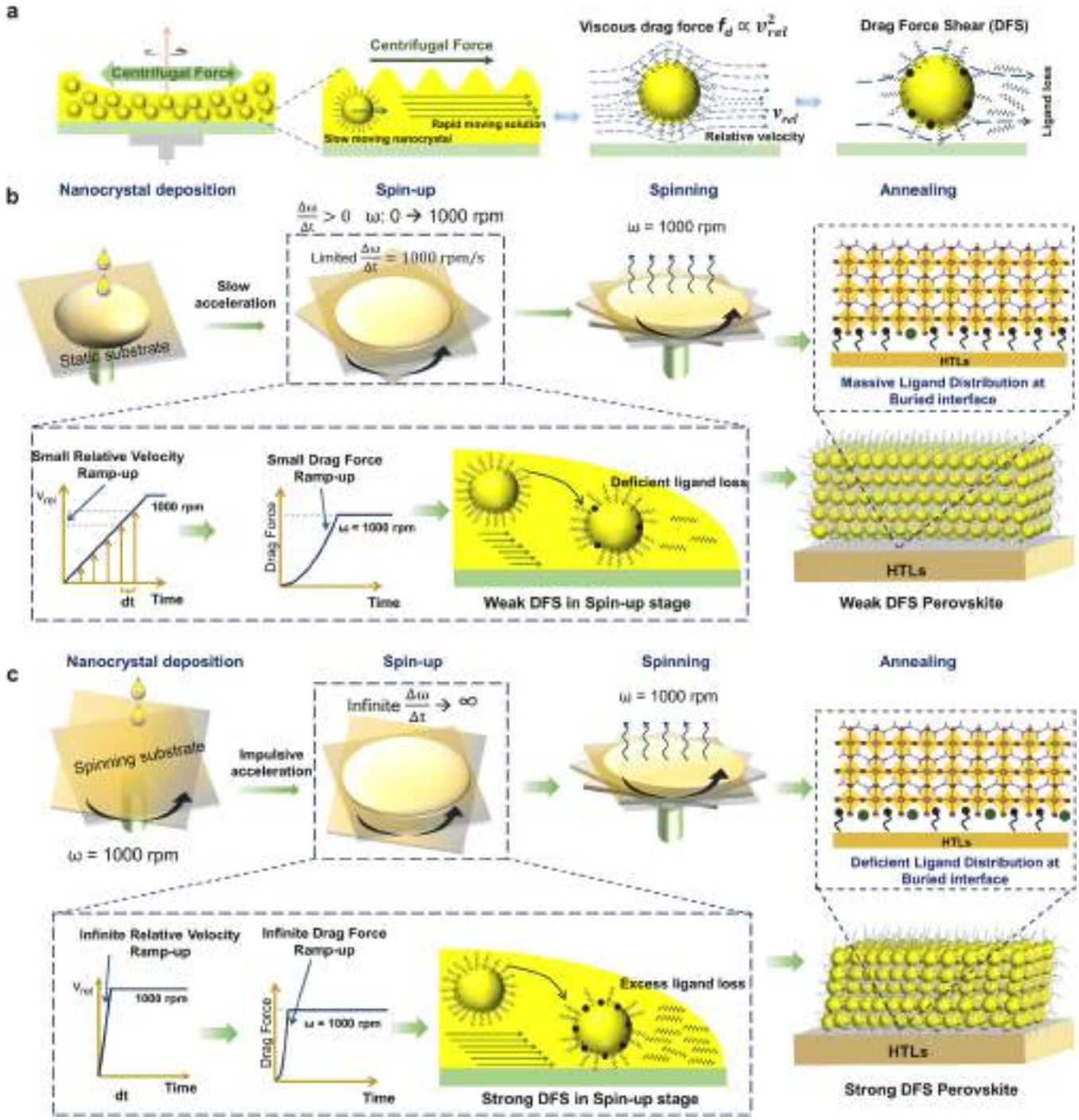

Fig. 1. Drag force shear (DFS) manipulating ligand distribution at buried interface. (a) Schematic diagram of drag force between solution and nanocrystals and corresponding drag force shear (DFS) during spin coating process. (b) Fabrication process of weak DFS perovskite. (c) Fabrication process of strong DFS perovskite.

carrier injection barrier lead by less ligand distribution at the buried interface. In this regard, an optimized DFS was employed to effectively balance the carrier injection barrier and defect passivation at the buried interface. Consequently, the optimal DFS processed PeLED exhibits an obviously suppressed EQE roll-off with higher peak EQE of 17.25 %, leading to a remarkable luminance of 61,900 cd/m^2. This work provides important insights in understanding and manipulating the ligand distribution at perovskite buried interface for achieving high-performance PeLEDs with suppressed EQE roll-off.

2. Results and discussions

Fig. 1 schematically demonstrated the drag force shear (DFS) manipulates the ligand distribution at perovskite buried interface. As shown in Fig. 1a, during the spin coating process, the perovskite nanocrystal solution will diffuse outward under centrifugal force. However, the solvent will rapidly diffuse due to its rheology, and the nanocrystals inside will move much slowly due to their heavier weight. This leads to the solvent rapidly flowing through the surface of the nanocrystals, resulting in a viscous drag force between the rapidly flowing solvent and the nanocrystals. As shown in Fig. S2, the nanocrystals mainly exhibit spherical shapes with an average radius of 8.4 nm. In this case, the viscous drag force should be evaluated by [43–46]:

$$f_d = \frac{1}{2} C_D \rho_f v_{rel}^2 A_s \quad (1)$$

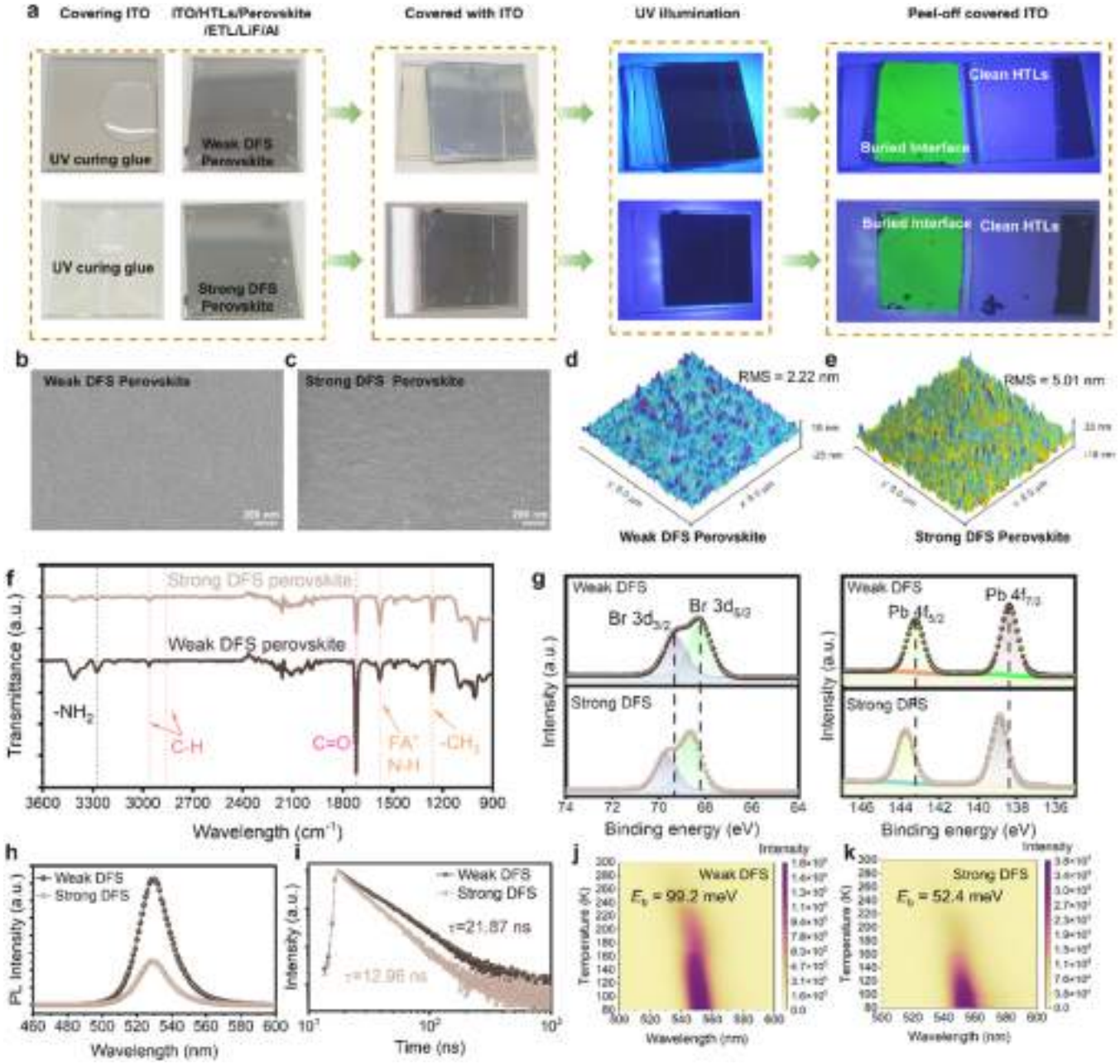

Fig. 2. Ligand distributions of perovskite buried interfaces. (a) Peel-off procedures of weak DFS perovskite buried interfaces (upper) and strong DFS perovskite buried interface (down). (b, c) SEM images of (b) weak DFS and (c) strong DFS perovskite buried interface. (d, e). The AFM images of (d) weak DFS and (e) strong DFS perovskite buried interface. (f–i) FTIR characterizations (f), X-ray photoelectron spectroscopy (XPS) spectra (g), photoluminescence (PL) spectra (h) and Time-resolved PL (TRPL) spectra (i) of perovskite buried interfaces. (j, k). The temperature-dependent PL maps for (j) weak DFS and (k) strong DFS perovskite buried interface.

where ρ_f is the density of liquid solution (toluene); C_D is the drag coefficient, which strongly dependents on Reynold's number thus can be considered as a constant for laminar flow condition [47,48], A_s is the surface of particle; and v_{rel} is superficial fluid-particle relative (slip) velocity. Obviously, the f_d is determined by the solution slip velocity v_{rel}. As mentioned above, the combination between surface ligands and nanocrystal are dynamic and weak binding. Thus, the surface ligands would be easily sheared by a greater viscous drag in spin-coating process. Resultantly, the perovskite film will lose surface ligand during the film-deposition process.

In this regard, we designed the different intensity of drag force shear to manipulate the ligand distribution at the perovskite buried interface. As shown in Fig. 1b, Fig. S1 and Supplementary Note 1, if the solution is slowly accelerated with a limited spin acceleration $\frac{\Delta\omega}{\Delta t} = 1000\,rpm/s$, there will be a slowly solvent acceleration through the nanocrystals, leading to a weak DFS to the nanocrystal. This would significantly preserve the surface ligand from nanocrystal, resulting in massive ligand distribution at buried interface for weak DFS perovskite. On the contrary, if the substrate has already rotated at 1000 rpm during the deposition of the nanocrystal solution, the solvent will impulsively accelerate under tremendous centrifugal force, causing a significant loss of surface ligands under strong DFS. Therefore, there will be deficient ligand distribution at the buried interface for strong DFS perovskite.

To verify the influence of DFS on the ligand distribution at buried interface, we directly peeled-off and characterized the perovskite buried interface following by the procedure illustrated in Fig. 2a and Experimental details. We firstly conducted various FTIR characterizations to confirm the successfully peeling-off of the buried interface. As shown in Fig. S3, the peeled-off buried interface exhibit no overlap with characteristic peaks of the hole-transporting layer (HTL) substrate. Instead, they closely align with signals from the perovskite nanocrystal solution and the upper surface of the perovskite film, confirming the successful peeling of a pristine perovskite buried interface without substrate residuals. The plane scanning electron microscopy (SEM) images image shows that DFS has only a minimal impact on the nanocrystal packing at the buried interface (Fig. 2b, c). However, the buried interface of the strong DFS perovskite exhibits greater surface roughness, which is consistent with the results obtained from atomic force microscopy (AFM). As shown in Fig. 2d, e, the surface roughness of the strong DFS perovskite buried interface (RMS = 2.22 nm) is significantly lower than that of the weak DFS perovskite buried interface (RMS = 5.01 nm). As shown in Fig. 2f, the FTIR signal of weak DFS perovskite buried interface is much stronger than that of strong DFS perovskite buried interface. Considering that the crystal structure and the thickness of perovskite film is immune of the DFS (Fig. S4, S5), the stronger FTIR signal of weak DFS perovskite interface should be attributed to its better ligand preservation. This clearly confirms that a weaker DFS would significantly increase ligand distribution at perovskite buried interface. The X-ray photoelectron spectroscopy (XPS) spectra show that the characteristic peaks of Pb $4f_{5/2}$ and $4f_{7/2}$ in weak DFS perovskite buried interface experience a substantial shift to lower binding energy than those in strong DFS perovskite buried interface. The same phenomenon is observed for Br $3d_{3/2}$ and $3d_{5/2}$. Negative Pb 4*f* binding energy shifts indicate a decrease in cationic charge on Pb^{2+} ions, which can be attributed to the richer electron-donating from ligands to the uncoordinated Pb^{2+} [49,50], indicating a better ligand preservation of weak DFS perovskite buried interface (Fig. 2g). The negative shifts of Br 3*d* binding energy should be attributed to the disturbed static interactions between Pb^{2+} and Br^- ions due to electron donation from ligands to the Pb^{2+} ions [51]. Both FTIR spectra and XPS spectra demonstrated the denser ligand distribution of weak DFS perovskite at buried interface.

The ligand distribution at buried interface will greatly influence the photo-physics characteristic of perovskite film. As shown in Fig. 2h, i, the weak DFS perovskite buried interface exhibits a much stronger PL intensity and an obviously longer PL lifetime than those of strong DFS perovskite buried interface, indicating the less surface defect at weak DFS perovskite buried interface [52]. Generally, the exciton binding energy (E_b) can estimate the barriers for exciton dissociation or exciton annihilation by non-radiative centers [53,54]. Here, the E_b was extracted from temperature-dependent PL spectra by Arrhenius equation [55]:

$$I(T) = \frac{I_0}{1 + Aexp\left(-\frac{E_b}{k_B T}\right)} \quad (2)$$

where, I(T) is the integral temperature dependent PL intensity, I_0 is the PL intensity at 0 K, A is a constant and k_B is Boltzmann constant. As demonstrated, the weak DFS perovskite buried interface demonstrates a much greater E_b of 99.2 meV than that of strong DFS perovskite buried interface (52.4 meV), demonstrating a much higher energy threshold for exciton thermal dissociation or annihilation by non-radiation centers in weak DFS perovskite buried interface (Fig. 2j,k and Fig. S6) [56], which can significantly reduce the non-radiative recombination of weak DFS perovskite. Therefore, the radiative recombination of the weak DFS perovskite should be significantly improved, which has been proved the much higher PLQY of the weak DFS perovskite (69.3 %) than the strong DFS perovskite film of 25.9 % (Fig. S7). Based on the analysis of FTIR, PL and TRPL, we can contribute the significantly reduced non-radiative recombination of weak DFS perovskite to the reduced defect state density [57], indicating the better defect passivation by surface ligand. Consequently, these observations serve as supplementary evidence affirming that a stronger DFS will enhance the ligand loss during the film deposition, resulting in deficient ligand distribution at perovskite buried interface.

Unfortunately, the passivating ligand usually are electrically insulating. Although a denser ligand distribution will evidently reduce the surface defect, it would also create a huge barrier for carrier injection at the buried interface. The Kelvin potential force microscopy (KPFM) measurement and ultraviolet photoelectron spectroscopy (UPS) test at the perovskite/HTL interface are performed to identify the carrier injection barrier (Fig. 3 and Fig. S8). As illustrated in Fig. 3a–e, the surface potential difference between the weak DFS perovskite and HTLs (150 mV) is evidently larger than that between the strong DFS perovskite and HTLs (67 mV), indicating a greater Fermi level difference between weak DFS perovskite and HTLs [58]. The UPS spectra show that valance band maximum (VBM) of both buried interfaces are deeper than HTLs, indicating a barrier for hole injection from HTLs to perovskite (Fig. S8). The weak DFS perovskite buried interface possesses a deeper VBM than strong DFS perovskite buried interface, demonstrating that there is a greater hole injection barrier at weak DFS perovskite buried interface. As shown in Figs. 2f and 2g, we performed the SCLC characterizations on hole-only devices. Interestingly, the SCLC of weak DFS perovskite-based hold-only device (HOD) shows a lower current density with a smaller V_{TFL} than those of infinite perovskite based HOD. The lower current density indicates the more difficult for carrier injection, confirming the greater carrier injection barrier caused by the excessive ligand distribution at weak DFS perovskite buried interface. Meanwhile, the smaller V_{TFL} demonstrates a lower defect density in weak DFS perovskite [59], which is consistent with the former results.

The PeLEDs were fabricated to reveal the effects of DFS process on device performances (Fig. 4a and Fig. S9). As illustrated in Fig. 4b, the weak DFS perovskite based PeLEDs (abbreviated as weak DFS PeLED) demonstrated a much lower current-density (J) than that of strong DFS perovskite based PeLEDs (abbreviated as strong DFS PeLED), which is

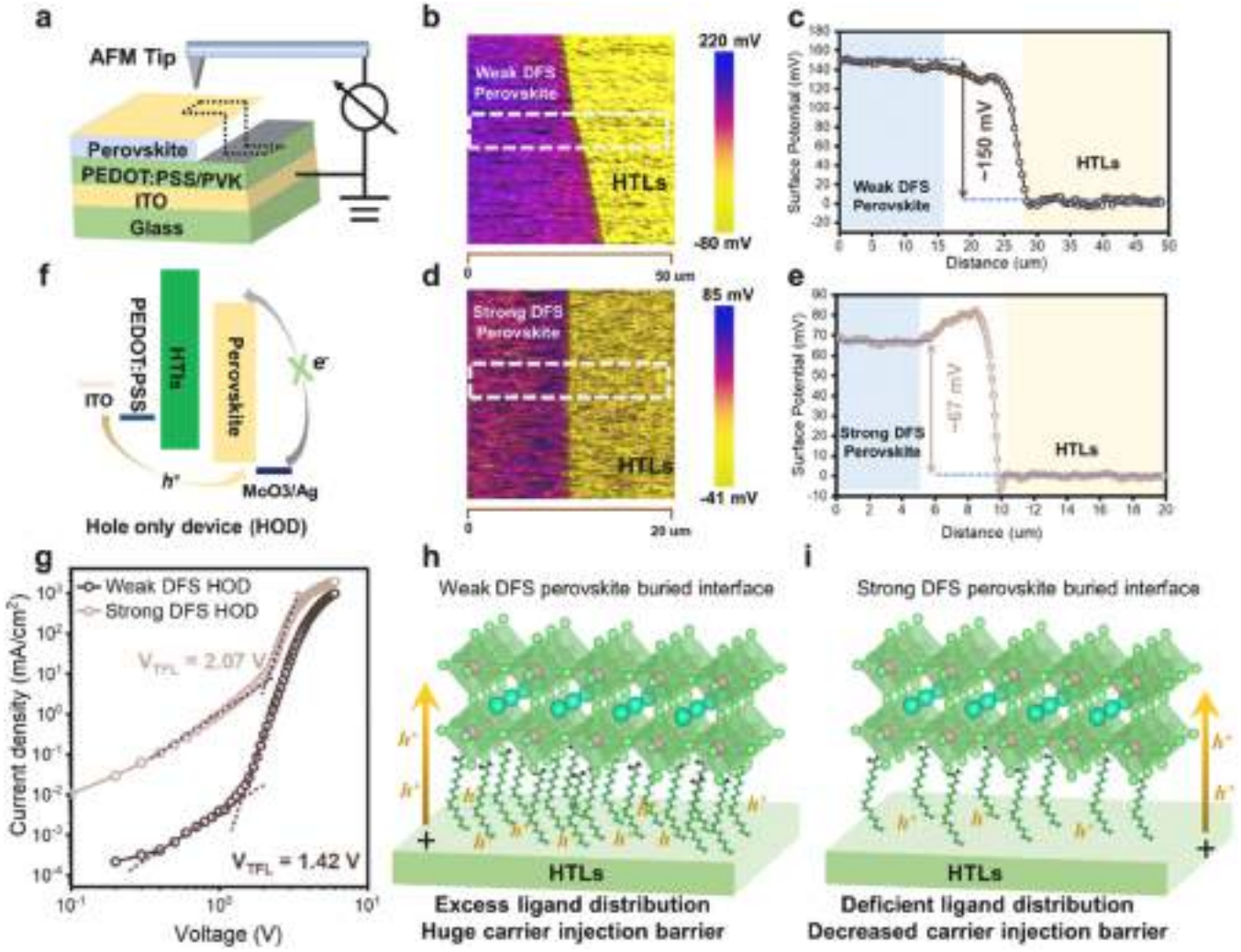

Fig. 3. The carrier injection barrier at perovskite buried interface. (a) The schematic diagram of Kelvin potential force microscopy (KPFM) measurement of the perovskite/HTL interface, the dashed lines represent the measured area. (b) The KPFM image and (c) corresponding surface potential of weak DFS perovskite/HTL interface. (d) The KPFM image and (e) corresponding surface potential of strong DFS perovskite/HTL interface. (f) The device structure of hole-only device (HOD). (g) The SCLC characterizations of weak DFS perovskite based and strong DFS perovskite based HOD. (h, i) The schematic diagram of the relationship between the ligand distribution and the carrier injection barrier at (h) weak DFS perovskite buried interface and (i) strong DFS perovskite buried interface.

consistent with the higher hole-injection barrier at weak DFS perovskite buried interface. As shown in Figs. 4c and 4d, the weak DFS PeLED exhibits a higher luminance than strong DFS PeLED at a small current density lower than 9 mA/cm^2. This brings about a much higher EQE of weak DFS PeLED (14.42 %) than that of strong DFS PeLED (9.38 %). The higher EQE of weak DFS PeLED should be attributed to the better radiative recombination of weak DFS perovskite due to the better surface defect passivation. However, at a high current density greater than 10 mA/cm^2, the weak DFS PeLEDs demonstrates a lower luminance and a faster luminance decay than strong DFS PeLEDs, which causes a lower peak luminance and a severer EQE roll-off for weak DFS PeLEDs (Fig. 4e, f).

The low-frequency capacitance-voltage (C-V) curves and its corresponding dC/dV curves were performed to unrevealing the carrier injection, recombination, and accumulation processes in PeLED devices [60,61], as shown in Fig. 4g, h. The capacitance of PeLEDs at different voltage can be quantified by following expression [60,62]:

$$C = \frac{dQ_{inj} + dQ_{trapped} - dQ_{recom}}{dV} \quad (3)$$

where dQ_{inj}, $dQ_{trapped}$ and dQ_{recom} are the injected, trapped and recombined charges. The dC/dV curve can be obtained by differentiating the C-V curves, which can efficiently reveal following five regions: dark current region, injection and weak recombination region, injection and recombination region, strong recombination region and recombination and accumulation region [59,61]. As shown in Fig. 4g, the capacitance of the weak DFS PeLED rapidly decreases after 5.33 V, while the capacitance of the strong DFS PeLED starts to slowly decrease after 6.39 V. The rapid decrease in capacitance indicates strong carrier radiative recombination within the weak DFS PeLED. However, Fig. 4h shows that the dC/dV - V curves of weak DFS PeLED demonstrates a noticeable protrusion in the strong-recombination range, indicating a fast carrier accumulation despite the strong carrier recombination [61]. Such a fast carrier accumulation should be ascribed to the great carrier injection barrier at buried interface due to the massive ligand preservation at the buried interfaces. As a result, the current density of strong DFS PeLED cannot be increased and its EQE is rapidly decreased under a high current density.

As demonstrated above, the key to obtaining a high-performance

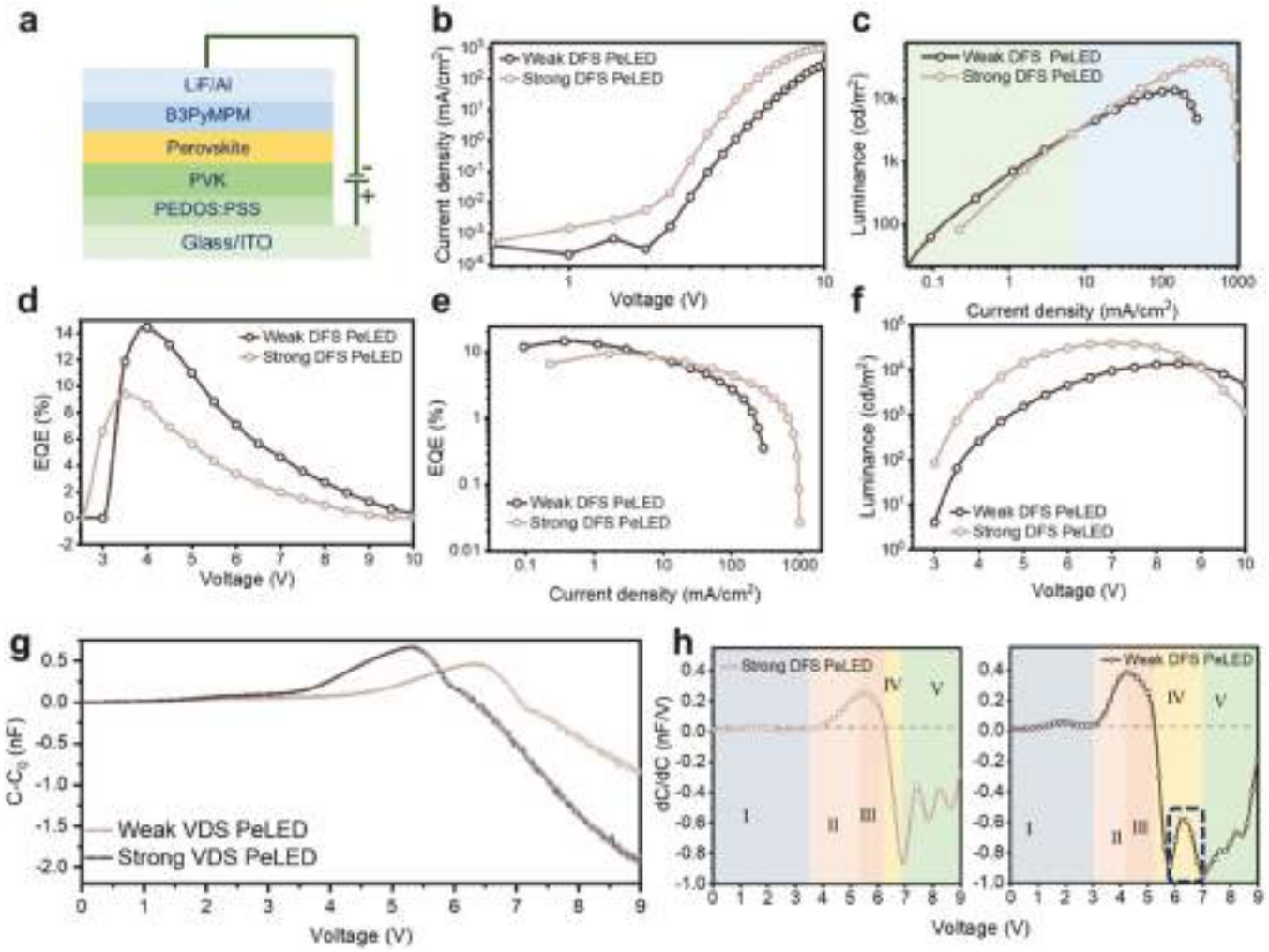

Fig. 4. The performances of PeLEDs. (a) Schematic diagrams of device structures. (b-f). (b) Current density-voltage (J-V) curves, (c) Current density-luminance (J-L) curves, (d) EQE-voltage curves, (e) The EQE roll-off curves and (f) luminance-voltage curves of PeLED. (g) The low-frequency (f = 5 K) capacitance-voltage (C-V) curves and (h) corresponding dC/dV curves of PeLEDs. The dC/dV- V curves can be divided into five regions: I, dark current region; II: injection & weak recombination region; III, injection & recombination region, IV, strong recombination region; V, recombination & accumulation region.

PeLED with a suppressed EQE roll-off lies in achieving a balance between the carrier injection barrier and defect passivation through the manipulation of ligand distribution at the perovskite buried interface. Fortunately, the DFS presents an avenue for fine-tuning the ligand distribution at the perovskite buried interface. In this regard, an optimal DFS ($\frac{\Delta\omega}{\Delta t} = 10000\ rpm/s$) was employed to optimize the ligand distribution at perovskite buried interface to balance carrier injection barrier and defect passivation at the buried interface (Fig. 5a, Fig. S10, S11).

As shown in Fig. 5c, the current density of optimal DFS PeLED has been obviously increased, indicating a significantly reduced carrier injection barrier at buried interface. The peak EQE of the optimal DFS PeLED device increases from 14.42 % to 17.25 %, substantiating that rational balance between the carrier injection carrier and defect passivation can improve device performance (Fig. 5e). With this balanced carrier injection and defect passivation, the luminance of the optimal DFS PeLED has increased from 1.35×10^5 cd/m^2 to 6.19×10^5 cd/m^2 compared with weak DFS PeLED (Fig. 5d). Comparing with the weak DFS PeLED, the C-V curve of optimal DFS PeLED in strong recombination region drops much faster, however, the low-frequency dC/dV–V curves demonstrates that there is no obvious dC/dV protrusion in optimal DFS PeLED at strong recombination range, proving that the successfully relieved carrier accumulation in device (Fig. 5j, i). Consequently, the equilibrium achieved between the carrier injection barrier and defect passivation at the perovskite buried interface resulted in an improved device performance while concurrently suppressing EQE roll-off in the optimal DFS PeLED (Fig. 5f, g).

3. Conclusion

In summary, we have demonstrated that drag force from the relative motion between solvent and nanocrystal can effectively modulate the ligand distribution at the perovskite buried interface during the spin-coating acceleration stage by shearing the surface ligand, thereby achieving high-performance PeLEDs with suppressed EQE roll-off. Through manipulating the ligand distribution at the perovskite buried interface, the relationships between the performance of PeLEDs (EQE and EQE roll-off) and ligand preservation at the buried interface are clearly revealed. In comparison with the strong drag force shear (DFS),

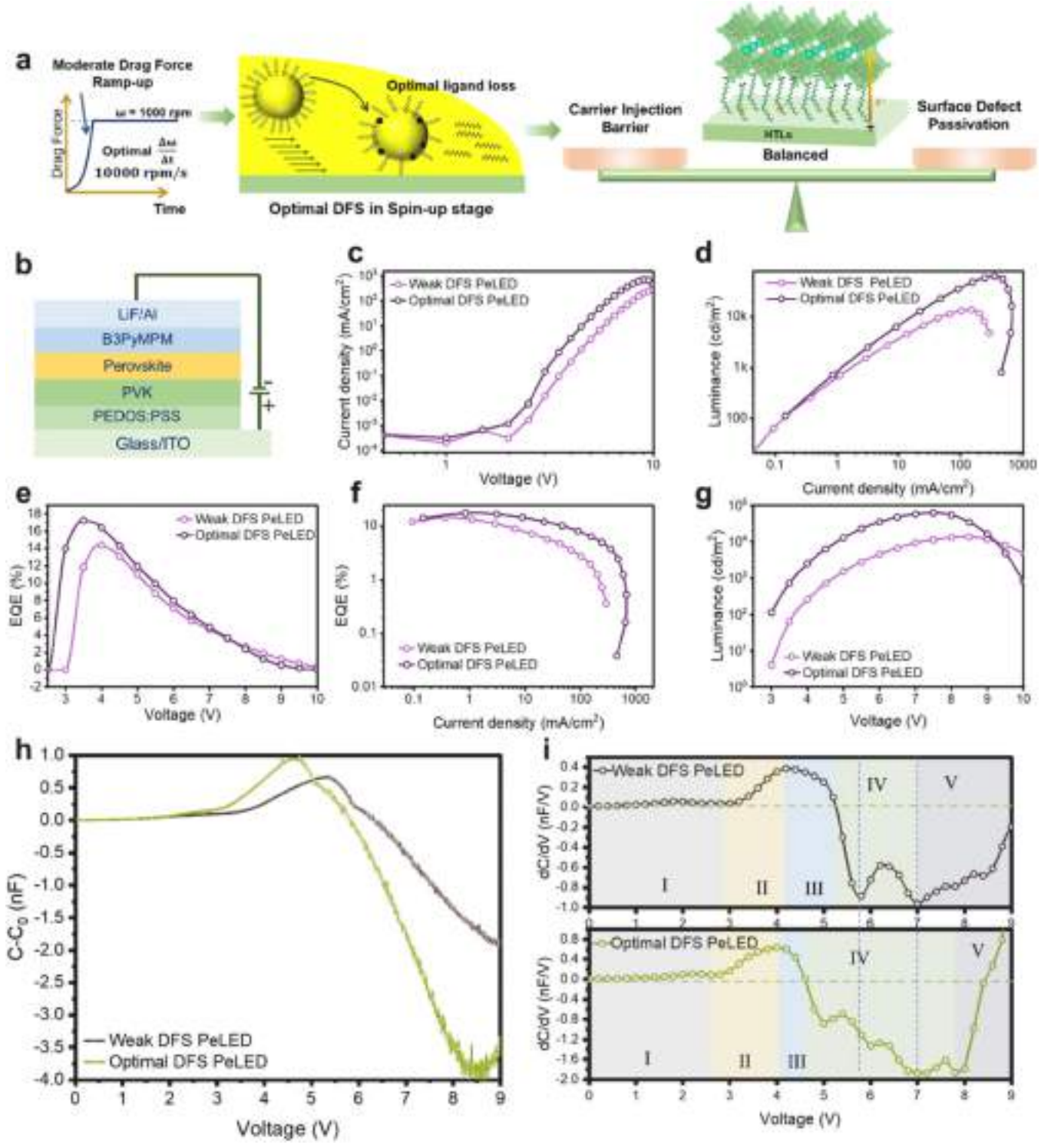

Fig. 5. Optimizing ligand distribution at buried interface for suppressed EQE roll-off of higher-performance PeLEDs. (a) Schematic illustration of balancing the carrier injection carrier and surface defect passivation by manipulating the ligand distribution through a moderate DFS. (b) device structure of PeLEDs. (c) J-V curves, (d) L-J curves, (e) EQE-voltage curves, (f) EQE roll-off curves and (g) luminance-voltage curves of weak DFS PeLED and optimal DFS PeLED. (h) The low-frequency C-V curves and (i) corresponding dC/dV – V curves of weak DFS PeLED and optimal DFS PeLED.

the weak DFS is capable of effectively decreasing interfacial defects of perovskite by increasing the ligand distribution at the buried interface. However, this simultaneously leads to an increase of the carrier injection barrier at the buried interface. Consequently, the weak DFS can achieve a higher EQE, while it also results in a rapid EQE roll-off in PeLED devices. Based on this understanding, an optimal DFS was employed to effectively balance defect passivation and the injection barrier at the buried interface. Resultantly, optimal DFS PeLED devices could effectively alleviate the rapid EQE roll-off observed in weak DFS PeLED with an enhanced EQE. Eventually, the optimal DFS PeLED achieved a

remarkable EQE of 17.24 % and a high luminance of 61,900 cd/m^2. This work highlights a simple yet effective strategy of controlling the ligand distribution at the buried interface, providing crucial insights for achieving high luminance and commercialization in nanocrystal based PeLEDs.

CRediT authorship contribution statement

Lunyao Pan: Validation. **Yongjian Chen:** Writing – review & editing, Validation. **Xiangrong Chen:** Supervision, Funding acquisition. **Guanqi Tang:** Writing – review & editing, Writing – original draft, Supervision, Conceptualization. **Xiaodong Peng:** Investigation, Data curation, Conceptualization. **Qungui WANG:** Writing – review & editing, Writing – original draft, Visualization, Validation, Methodology, Investigation, Formal analysis, Data curation, Conceptualization. **Xiankan Zeng:** Validation, Conceptualization. **Wen Li:** Resources, Funding acquisition, Formal analysis. **Weiqing Yang:** Writing – review & editing, Supervision, Resources, Methodology, Funding acquisition.

Declaration of Competing Interest

The authors declare no competing financial interest or personal relationships that would influence this work.

Data availability

Data will be made available on request.

Acknowledgments

This work was financially supported by the National Natural Science Foundation of China (Grant nos. 12074274 and 52202188).

Appendix A. Supporting information

Supplementary data associated with this article can be found in the online version at doi:10.1016/j.nanoen.2024.109797.

References

[1] A. Liu, C. Bi, J. Li, M. Zhang, C. Cheng, D. Binks, J. Tian, High color-purity and efficient pure-blue perovskite light-emitting diodes based on strongly confined monodispersed quantum dots, Nano Lett. 23 (2023) 2405–2411, https://doi.org/10.1021/acs.nanolett.3c00548.

[2] Z. Yao, C. Bi, A. Liu, M. Zhang, J. Tian, High brightness and stability pure-blue perovskite light-emitting diodes based on a novel structural quantum-dot film, Nano Energy 95 (2022) 106974, https://doi.org/10.1016/j.nanoen.2022.106974.

[3] J.S. Kim, J.-M. Heo, G.-S. Park, S.-J. Woo, C. Cho, H.J. Yun, D.-H. Kim, J. Park, S.-C. Lee, S.-H. Park, E. Yoon, N.C. Greenham, T.-W. Lee, Ultra-bright, efficient and stable perovskite light-emitting diodes, Nature 611 (2022) 688–694, https://doi.org/10.1038/s41586-022-05304-w.

[4] X. Shi, J. Zhang, L. Kong, L. Wang, Y. Dou, S. Wang, W. Li, X. Zhang, L. Yan, X. Yang, A mixed solvent strategy enabling efficient all-solution-processed perovskite light-emitting diodes, J. Mater. Chem. C 10 (2022) 8964–8971, https://doi.org/10.1039/D2TC01201D.

[5] S. Chu, Y. Zhang, P. Xiao, W. Chen, R. Tang, Y. Shao, T. Chen, X. Zhang, F. Liu, Z. Xiao, Large-area and efficient sky-blue perovskite light-emitting diodes via blade-coating, Adv. Mater. 34 (2022) 2108939, https://doi.org/10.1002/adma.202108939.

[6] Y. Jiang, C. Sun, J. Xu, S. Li, M. Cui, X. Fu, Y. Liu, Y. Liu, H. Wan, K. Wei, T. Zhou, W. Zhang, Y. Yang, J. Yang, C. Qin, S. Gao, J. Pan, Y. Liu, S. Hoogland, E. H. Sargent, J. Chen, M. Yuan, Synthesis-on-substrate of quantum dot solids, Nature 612 (2022) 679–684, https://doi.org/10.1038/s41586-022-05486-3.

[7] J. Jiang, Z. Chu, Z. Yin, J. Li, Y. Yang, J. Chen, J. Wu, J. You, X. Zhang, Red perovskite light-emitting diodes with efficiency exceeding 25 % realized by co-spacer cations, Adv. Mater. 34 (2022) 2204460, https://doi.org/10.1002/adma.202204460.

[8] W. Bai, T. Xuan, H. Zhao, H. Dong, X. Cheng, L. Wang, R.-J. Xie, Perovskite light-emitting diodes with an external quantum efficiency exceeding 30 %, Adv. Mater. 35 (2023) 2302283 https://doi.org/10.1002/adma.202302283.

[9] W. Zhou, Y. Shen, L.-X. Cao, Y. Lu, Y.-Y. Tang, K. Zhang, H. Ren, F.-M. Xie, Y.-Q. Li, J.-X. Tang, Manipulating ionic behavior with bifunctional additives for efficient sky-blue perovskite light-emitting diodes, Adv. Funct. Mater. 33 (2023) 2301425, https://doi.org/10.1002/adfm.202301425.

[10] T.-H. Han, K.Y. Jang, Y. Dong, R.H. Friend, E.H. Sargent, T.-W. Lee, A roadmap for the commercialization of perovskite light emitters, Nat. Rev. Mater. 7 (2022) 757–777, https://doi.org/10.1038/s41578-022-00459-4.

[11] A. Fakharuddin, M.K. Gangishetty, M. Abdi-Jalebi, S.-H. Chin, A.R. bin Mohd Yusoff, D.N. Congreve, W. Tress, F. Deschler, M. Vasilopoulou, H.J. Bolink, Perovskite light-emitting diodes, Nat. Electron. 5 (2022) 203–216, https://doi.org/10.1038/s41928-022-00745-7.

[12] X.-K. Liu, W. Xu, S. Bai, Y. Jin, J. Wang, R.H. Friend, F. Gao, Metal halide perovskites for light-emitting diodes, Nat. Mater. 20 (2021) 10–21, https://doi.org/10.1038/s41563-020-0784-7.

[13] W.H. Jeong, S. Lee, H. Song, X. Shen, H. Choi, Y. Choi, J. Yang, J.W. Yoon, Z. Yu, J. Kim, G.E. Seok, J. Lee, H.Y. Kim, H.J. Snaith, H. Choi, S.H. Park, B.R. Lee, Synergistic surface modification for high-efficiency perovskite nanocrystal light-emitting diodes: divalent metal ion doping and halide-based ligand passivation, Adv. Sci., n/a, 2305383. ⟨https://doi.org/10.1002/advs.202305383⟩.

[14] T. Chiba, Y. Hayashi, H. Ebe, K. Hoshi, J. Sato, S. Sato, Y.-J. Pu, S. Ohisa, J. Kido, Anion-exchange red perovskite quantum dots with ammonium iodine salts for highly efficient light-emitting devices, Nat. Photonics 12 (2018) 681–687, https://doi.org/10.1038/s41566-018-0260-y.

[15] A. Pan, B. He, X. Fan, Z. Liu, J.J. Urban, A.P. Alivisatos, L. He, Y. Liu, Insight into the ligand-mediated synthesis of colloidal CsPbBr3 perovskite nanocrystals: the role of organic acid, base, and cesium precursors, ACS Nano 10 (2016) 7943–7954, https://doi.org/10.1021/acsnano.6b03863.

[16] W. Yin, M. Li, W. Dong, X. Zhang, W. Zheng, Overcoming the ambient manufacturability-performance bottleneck in perovskite nanocrystal emitters for efficient light-emitting diodes, Angew. Chem. Int. Ed. 62 (2023) e202303462, https://doi.org/10.1002/anie.202303462.

[17] W. Zheng, Q. Wan, M. Liu, Q. Zhang, C. Zhang, R. Yan, X. Feng, L. Kong, L. Li, CsPbBr3 nanocrystal light-emitting diodes with efficiency up to 13.4 % achieved by careful surface engineering and device engineering, J. Phys. Chem. C 125 (2021) 3110–3118, https://doi.org/10.1021/acs.jpcc.0c11085.

[18] M.-G. Jeon, A. Kirakosyan, C. Shin, S. Yun, J. Kim, L. Li, J. Choi, Overcoming charge transfer barriers via electrostatically stabilized CsPbBr3 nanocrystals for efficient perovskite light-emitting diodes, Chem. Eng. J. 462 (2023) 142120, https://doi.org/10.1016/j.cej.2023.142120.

[19] H. Li, W. Dong, X. Shen, C. Ge, Y. Song, Z. Wang, A. Wang, Z. Yang, M. Hao, Y. Zhang, W. Zheng, X. Zhang, Q. Dong, Enhancing the efficiency and stability of CsPbI3 nanocrystal-based light-emitting diodes through ligand engineering with octylamine, J. Phys. Chem. C 126 (2022) 1085–1093, https://doi.org/10.1021/acs.jpcc.1c10115.

[20] S. Kumar, J. Jagielski, T. Marcato, S.F. Solari, C.-J. Shih, Understanding the ligand effects on photophysical, optical, and electroluminescent characteristics of hybrid lead halide perovskite nanocrystal solids, J. Phys. Chem. Lett. 10 (2019) 7560–7567, https://doi.org/10.1021/acs.jpclett.9b02950.

[21] Y.-H. Kim, G.-H. Lee, Y.-T. Kim, C. Wolf, H.J. Yun, W. Kwon, C.G. Park, T.W. Lee, High efficiency perovskite light-emitting diodes of ligand-engineered colloidal formamidinium lead bromide nanoparticles, Nano Energy 38 (2017) 51–58, https://doi.org/10.1016/j.nanoen.2017.05.002.

[22] K. Hills-Kimball, H. Yang, T. Cai, J. Wang, O. Chen, Recent advances in ligand design and engineering in lead halide perovskite nanocrystals, Adv. Sci. 8 (2021) 2100214, https://doi.org/10.1002/advs.202100214.

[23] J. Li, L. Xu, T. Wang, J. Song, J. Chen, J. Xue, Y. Dong, B. Cai, Q. Shan, B. Han, H. Zeng, 50-Fold EQE improvement up to 6.27 % of solution-processed all-inorganic perovskite CsPbBr3 QLEDs via surface ligand density control, Adv. Mater. 29 (2017) 1603885, https://doi.org/10.1002/adma.201603885.

[24] T. Chiba, K. Hoshi, Y.-J. Pu, Y. Takeda, Y. Hayashi, S. Ohisa, S. Kawata, J. Kido, High-efficiency perovskite quantum-dot light-emitting devices by effective washing process and interfacial energy level alignment, ACS Appl. Mater. Interfaces 9 (2017) 18054–18060, https://doi.org/10.1021/acsami.7b03382.

[25] J. Ye, M.M. Byranvand, C.O. Martínez, R.L.Z. Hoye, M. Saliba, L. Polavarapu, Defect Passivation in Lead-Halide Perovskite Nanocrystals and Thin Films: Toward Efficient LEDs and Solar Cells, vol. 60, 2021, pp. 21636–60. ⟨https://doi.org/10.1002/anie.202102360⟩.

[26] L. Gao, T. Cheng, L. Gou, Y. Zhang, Y. Liu, L. Yuan, X. Zhang, Y. Wang, F. Meng, J. Zhang, Eliminating nanocrystal surface light loss and ion migration to achieve bright mixed-halide blue perovskite LEDs, ACS Appl. Mater. Interfaces 15 (2023) 18125–18133, https://doi.org/10.1021/acsami.3c02437.

[27] Y. Zhang, L. Chouhan, E. Fron, L. Leoncino, K. Elkhouly, H. Bhatia, W. Qiu, M.B. J. Roeffaers, J. Hofkens, E. Debroye, B. Pradhan, Operationally stable and efficient CsPbI3–xBrx perovskite nanocrystal light-emitting diodes enabled by ammonium ligand surface treatment, ACS Photonics 10 (2023) 2774–2783, https://doi.org/10.1021/acsphotonics.3c00480.

[28] Y. Hassan, J.H. Park, M.L. Crawford, A. Sadhanala, J. Lee, J.C. Sadighian, E. Mosconi, R. Shivanna, E. Radicchi, M. Jeong, C. Yang, H. Choi, S.H. Park, M. H. Song, F. De Angelis, C.Y. Wong, R.H. Friend, B.R. Lee, H.J. Snaith, Ligand-engineered bandgap stability in mixed-halide perovskite LEDs, Nature 591 (2021) 72–77, https://doi.org/10.1038/s41586-021-03217-8.

[29] J.H. Park, A.-y Lee, J.C. Yu, Y.S. Nam, Y. Choi, J. Park, M.H. Song, Surface Ligand Engineering for Efficient Perovskite Nanocrystal-Based Light-Emitting Diodes, ACS Appl. Mater. Interfaces, vol. 11, 2019, pp. 8428–35. ⟨https://doi.org/10.1021/acsami.8b20808⟩.

[30] Y. Dong, Y.-K. Wang, F. Yuan, A. Johnston, Y. Liu, D. Ma, M.-J. Choi, B. Chen, M. Chekini, S.-W. Baek, L.K. Sagar, J. Fan, Y. Hou, M. Wu, S. Lee, B. Sun, S. Hoogland, R. Quintero-Bermudez, H. Ebe, P. Todorovic, F. Dinic, P. Li, H. T. Kung, M.I. Saidaminov, E. Kumacheva, E. Spiecker, L.-S. Liao, O. Voznyy, Z.-H. Lu, E.H. Sargent, Bipolar-shell resurfacing for blue LEDs based on strongly

confined perovskite quantum dots, Nat. Nanotechnol. 15 (2020) 668–674, https://doi.org/10.1038/s41565-020-0714-5.
[31] N.K. Kumawat, A. Swarnkar, A. Nag, D. Kabra, Ligand engineering to improve the luminance efficiency of CsPbBr3 nanocrystal based light-emitting diodes, J. Phys. Chem. C 122 (2018) 13767–13773, https://doi.org/10.1021/acs.jpcc.8b00723.
[32] Y.-H. Kim, J. Park, S. Kim, J.S. Kim, H. Xu, S.-H. Jeong, B. Hu, T.-W. Lee, Exploiting the full advantages of colloidal perovskite nanocrystals for large-area efficient light-emitting diodes, Nat. Nanotechnol. 17 (2022) 590–597, https://doi.org/10.1038/s41565-022-01113-4.
[33] Y. Wang, Y. Teng, P. Lu, X. Shen, P. Jia, M. Lu, Z. Shi, B. Dong, W.W. Yu, Y. Zhang, Low roll-off perovskite quantum dot light-emitting diodes achieved by augmenting hole mobility, Adv. Funct. Mater. 30 (2020) 1910140, https://doi.org/10.1002/adfm.201910140.
[34] A. Liu, C. Bi, J. Tian, All solution-processed high performance pure-blue perovskite quantum-dot light-emitting diodes, Adv. Funct. Mater. 32 (2022) 2207069, https://doi.org/10.1002/adfm.202207069.
[35] Y. Guo, S. Apergi, N. Li, M. Chen, C. Yin, Z. Yuan, F. Gao, F. Xie, G. Brocks, S. Tao, N. Zhao, Phenylalkylammonium passivation enables perovskite light emitting diodes with record high-radiance operational lifetime: the chain length matters, Nat. Commun. 12 (2021) 644, https://doi.org/10.1038/s41467-021-20970-6.
[36] W. Xiong, C. Zou, W. Tang, S. Xing, Z. Wang, B. Zhao, D. Di, Efficient and bright blue perovskite LEDs enabled by a carbazole-phosphonic acid interface, ACS Energy Lett. 8 (2023) 2897–2903, https://doi.org/10.1021/acsenergylett.3c00589.
[37] N. Fiuza-Maneiro, K. Sun, I. López-Fernández, S. Gómez-Graña, P. Müller-Buschbaum, L. Polavarapu, Ligand chemistry of inorganic lead halide perovskite nanocrystals, ACS Energy Lett. 8 (2023) 1152–1191, https://doi.org/10.1021/acsenergylett.2c02363.
[38] J. De Roo, M. Ibáñez, P. Geiregat, G. Nedelcu, W. Walravens, J. Maes, J.C. Martins, I. Van Driessche, M.V. Kovalenko, Z. Hens, Highly dynamic ligand binding and light absorption coefficient of cesium lead bromide perovskite nanocrystals, ACS Nano 10 (2016) 2071–2081, https://doi.org/10.1021/acsnano.5b06295.
[39] J. Park, H.M. Jang, S. Kim, S.H. Jo, T.-W. Lee, Electroluminescence of perovskite nanocrystals with ligand engineering, Trends Chem. 2 (2020) 837–849, https://doi.org/10.1016/j.trechm.2020.07.002.
[40] M.-G. Jeon, S. Yun, A. Kirakosyan, M.R. Sihn, S.-G. Yoon, J. Choi, Scale-up synthesis of organometal halide perovskite nanocrystals (MAPbX3, X = Cl, Br, and I), ACS Sustain. Chem. Eng. 7 (2019) 19369–19374, https://doi.org/10.1021/acssuschemeng.9b03153.
[41] H. Lee, J.W. Jeong, M.G. So, G.Y. Jung, C.-L. Lee, Design of chemically stable organic perovskite quantum dots for micropatterned light-emitting diodes through kinetic control of a cross-linkable ligand system, Adv. Mater. 33 (2021) 2007855, https://doi.org/10.1002/adma.202007855.
[42] T.-H. Le, S. Lee, E. Heo, U. Lee, H. Lee, H. Jo, K.S. Yang, M. Chang, H. Yoon, Controlled anisotropic growth of layered perovskite nanocrystals for enhanced optoelectronic properties, Chem. Eng. J. 416 (2021) 128045, https://doi.org/10.1016/j.cej.2020.128045.
[43] C.Q. LaMarche, B. Freireich, R. Cocco, J.W. Chew, Understanding drag part 1: well-established drag limits and homogeneous drag laws, Chem. Eng. J. 471 (2023) 144541, https://doi.org/10.1016/j.cej.2023.144541.
[44] J. Fu, K. Jiang, S. Chen, X. Du, Effect of large temperature difference on drag coefficient and Nusselt number of an ellipsoidal particle in compressible viscous flow, Powder Technol. 408 (2022) 117766, https://doi.org/10.1016/j.powtec.2022.117766.
[45] Y. Chen, P. Jiang, T. Xiong, W. Wei, Z. Fang, B. Wang, Drag and heat transfer coefficients for axisymmetric nonspherical particles: a LBM study, Chem. Eng. J. 424 (2021) 130391, https://doi.org/10.1016/j.cej.2021.130391.
[46] R. Ouchene, Numerical simulation and modeling of the hydrodynamic forces and torque acting on individual oblate spheroids, Phys. Fluids 32 (2020), https://doi.org/10.1063/5.0011618.
[47] W.R.A. Goossens, Review of the empirical correlations for the drag coefficient of rigid spheres, Powder Technol. 352 (2019) 350–359, https://doi.org/10.1016/j.powtec.2019.04.075.
[48] S.-J. Liao, An analytic approximation of the drag coefficient for the viscous flow past a sphere, Int. J. Non-Linear Mech. 37 (2002) 1–18, https://doi.org/10.1016/S0020-7462(00)00092-5.
[49] M. Yu, X. Mei, T. Qin, R. Zhuang, Y. Hua, X. Zhang, Modulating phase distribution and passivating surface defects of quasi-2D perovskites via potassium tetrafluoroborate for light-emitting diodes, Chem. Eng. J. 450 (2022) 138021, https://doi.org/10.1016/j.cej.2022.138021.
[50] L. Kong, X. Zhang, Y. Li, H. Wang, Y. Jiang, S. Wang, M. You, C. Zhang, T. Zhang, S. V. Kershaw, W. Zheng, Y. Yang, Q. Lin, M. Yuan, A.L. Rogach, X. Yang, Smoothing the energy transfer pathway in quasi-2D perovskite films using methanesulfonate leads to highly efficient light-emitting devices, Nat. Commun. 12 (2021) 1246, https://doi.org/10.1038/s41467-021-21522-8.
[51] B. Li, J. Zhen, Y. Wan, X. Lei, Q. Liu, Y. Liu, L. Jia, X. Wu, H. Zeng, W. Zhang, G.-W. Wang, M. Chen, S. Yang, Anchoring fullerene onto perovskite film via grafting pyridine toward enhanced electron transport in high-efficiency solar cells, ACS Appl. Mater. Interfaces 10 (2018) 32471–32482, https://doi.org/10.1021/acsami.8b11459.
[52] Z. Chu, Q. Ye, Y. Zhao, F. Ma, Z. Yin, X. Zhang, J. You, Perovskite Light-Emitting Diodes with External Quantum Efficiency Exceeding 22 % via Small-Molecule Passivation, vol. 33, 2021, 2007169. ⟨http://doi.org/10.1002/adma.202007169⟩.
[53] M. Leng, Y. Yang, Z. Chen, W. Gao, J. Zhang, G. Niu, D. Li, H. Song, J. Zhang, S. Jin, J. Tang, Surface passivation of bismuth-based perovskite variant quantum dots to achieve efficient blue emission, Nano Lett. 18 (2018) 6076–6083, https://doi.org/10.1021/acs.nanolett.8b03090.
[54] H. Cheng, Y. Feng, Y. Fu, Y. Zheng, Y. Shao, Y. Bai, Understanding and minimizing non-radiative recombination losses in perovskite light-emitting diodes, J. Mater. Chem. C 10 (2022) 13590–13610, https://doi.org/10.1039/D2TC01869A.
[55] X. Li, Y. Wu, S. Zhang, B. Cai, Y. Gu, J. Song, H. Zeng, CsPbX3 quantum dots for lighting and displays: room-temperature synthesis, photoluminescence superiorities, underlying origins and white light-emitting diodes, Adv. Funct. Mater. 26 (2016) 2435–2445, https://doi.org/10.1002/adfm.201600109.
[56] L. Zhou, J.-F. Liao, Y. Qin, X.-D. Wang, J.-H. Wei, M. Li, D.-B. Kuang, R. He, Activation of Self-Trapped Emission in Stable Bismuth-Halide Perovskite by Suppressing Strong Exciton–Phonon Coupling, 31, 2021, 2102654. ⟨https://doi.org/10.1002/adfm.202102654⟩.
[57] Z. Liu, W. Qiu, X. Peng, G. Sun, X. Liu, D. Liu, Z. Li, F. He, C. Shen, Q. Gu, F. Ma, H.-L. Yip, L. Hou, Z. Qi, S.-J. Su, Perovskite Light-Emitting Diodes with EQE Exceeding 28 % through a Synergetic Dual-Additive Strategy for Defect Passivation and Nanostructure Regulation, vol. 33, 2021, 2103268. ⟨https://doi.org/10.1002/adma.202103268⟩.
[58] Z. Kang, H. Si, M. Shi, C. Xu, W. Fan, S. Ma, A. Kausar, Q. Liao, Z. Zhang, Y. Zhang, Kelvin probe force microscopy for perovskite solar cells, Sci. China Mater. 62 (2019) 776–789, https://doi.org/10.1007/s40843-018-9395-y.
[59] Q. Wang, Y. Chen, C. Yan, X. Zeng, X. Fu, L. Pan, J. Cao, S. Yang, W. Li, X. Chen, W. Yang, Molecularly designing a passivation ETL to suppress EQE roll-off of PeLEDs, ACS Energy Lett. 8 (2023) 3710–3719, https://doi.org/10.1021/acsenergylett.3c01379.
[60] X. Xiao, T. Ye, J. Sun, X. Qu, Z. Ren, D. Wu, S. Ding, X.W. Sun, W.C.H. Choy, K. Wang, Capacitance–voltage characteristics of perovskite light-emitting diodes: modeling and implementing on the analysis of carrier behaviors, Appl. Phys. Lett. 120 (2022), https://doi.org/10.1063/5.0088231.
[61] J. Ma, H. Tang, X. Qu, G. Xiang, S. Jia, P. Liu, K. Wang, X.W. Sun, A dC/dV measurement for quantum-dot light-emitting diodes, Chin. Phys. Lett. 39 (2022) 128401, https://doi.org/10.1088/0256-307X/39/12/128401.
[62] X. Xiao, K. Wang, T. Ye, R. Cai, Z. Ren, D. Wu, X. Qu, J. Sun, S. Ding, X.W. Sun, W. C.H. Choy, Enhanced hole injection assisted by electric dipoles for efficient perovskite light-emitting diodes, Commun. Mater. 1 (2020) 81, https://doi.org/10.1038/s43246-020-00084-0.

Qungui Wang is currently pursuing his Ph.D degree from College of Physics, Sichuan University under the supervision of Prof. Xiangrong Chen and Prof. Weiqing Yang from Southwest Jiaotong University. He received his B.S. degree from College of Science, Northeast Forestry University in 2018. His interests include DFT calculations, perovskite optoelectronics and advanced photonics device.

Xiaodong Peng received his M.S. degree in Materials science from Southwest Jiaotong University in 2022. His research interests include perovskite luminescent material, quantum dot luminescence and physics of semiconductor devices.

Wen Li received her Ph.D. degree from the Lanzhou Institute of Chemical Physics, Chinese Academy of Science in 2017. She is currently an associate professor in the School of Materials Science and Engineering at Southwest Jiaotong University. Her research interests focus on optical materials, light-emitting diodes, solar cells, photoelectric detection and metal ion detection.

Xiankan Zeng received his M.S. in Materials Science and Engineering from Southwest Jiaotong University in 2022. He is currently pursuing Ph.D degree in Materials Science and Engineering at Southwest Jiaotong University. His main research interests are materials, devices and physics in optoelectronics.

Yongjian Chen is currently a postgraduate in the Southwest Jiaotong University under the supervision of Prof. Weiqing Yang. His current scientific research focuses on the construction and interface physics of efficient perovskite light-emitting diodes.

Lunyao Pan is Currently a postgraduate in the School of Materials Science and Engineering, Southwest Jiaotong University, under the supervision of Assoc. Prof. Wen Li and Prof. Weiqing Yang. His current scientific interests focus on novel inorganic hole transport layers for perovskite light-emitting diodes, interface physics.

Guanqi Tang received his PhD degree under the supervision of Prof. Yan Feng at the Department of Applied physics of the Hong Kong Polytechnic University in 2019. Now he is an associate professor at Research Institute of Frontier Science. His research interests are organic-inorganic halide perovskite based electronic devices.

Xiangrong Chen received his Ph.D degree in Atomic and Molecular Physics from Sichuan University in 1997. He worked as an associate professor in 1999 at Sichuan University. In 2000, he worked in Tsukuba University as a postdoctoral fellow. He returned to Sichuan University as a full professor in 2002. He is the academic and technical leaders in Sichuan Province, China. His scientific research has been focused on the atomic and molecular physics, including atomic and molecular clusters, high-pressure physics properties of materials and energetic materials.

Weiqing Yang received his M.S. and Ph.D degree from Sichuan University in 2007 and 2011, respectively. From 2011 to 2014, he worked as a postdoctoral researcher at the University of Electronic Science and Technology of China and the Georgia Institute of Technology. He joined the School of Materials Science and Technology at Southwest Jiaotong University as a professor and doctoral supervisor in April 2014. He is a highly cited Chinese scholar for many consecutive years. His research focuses on the application of nano energy materials and functional devices.